



Numerical study of upstream submerged vanes affecting bed in a sharp bend with a bridge pier via SSIIM software

Chonoor Abdi Chooplou¹ · Mohammad Vaghefi²

Received: 22 June 2023 / Accepted: 14 September 2023 / Published online: 1 October 2023
© Springer Nature Switzerland AG 2023

Abstract

Various protective measures are employed to alter flow patterns and mitigate the intensity of vortices and resulting scour around bridge piers. One such method involves the use of submerged vanes positioned upstream of the bridge piers. This study investigated the effects of the changes in the position of the submerged vanes across the channel, as well as distances of the vanes from the bridge pier and from each other with different 100, 50, and 0% overlapping lengths upstream of the pier in a sharp 180° bend by using a SSIIM numerical model. The results demonstrated that the SSIIM model accurately simulated scour with acceptable precision. The upstream submerged vanes significantly impacted the geometric characteristics of the scour cavity around the bridge pier, including maximum scour depth, scour cavity area, and scour cavity volume. On average, the scour depth and sedimentation were reduced by 15.67–50.60% and 6.53–20.41%, respectively. The vanes exhibited a more pronounced effect on reducing the scour cavity volume compared to its area with average reductions of 40.1 and 34.5%, respectively. Increasing the length of overlapping vanes by 50% resulted in a 62.5% reduction in the scour cavity length compared to that of the single-pier model. Additionally, the scour cavity slope was more symmetrical with upstream submerged vanes compared to the single-pier model.

Keywords Bed topography · Scour · Submerged vanes · 180-degree bend · SSIIM numerical model

Introduction

A strong helical flow occurring in curved open channels is the main feature of the flow. This helical flow mainly allows the lateral slope of the channel bed to be formed and developed and its shear stress to be distributed. The path of fluid particles and bed sediments depends on the power of the helical flow in the channel. Therefore, it is necessary that the effects of the helical flow for fluid particles and sediments be considered in the model in order to obtain an accurate numerical model of bed alterations in curved channels in rivers. In the past few years, numerous 3D models of flow pattern and sediments have been

developed by using more powerful calculation tools. A great number of researchers have so far made attempts to explore the pattern of the stream around bridge piers by means of experimental and numerical methods. Ye and McCorquodale [1] conducted a 3D hydrodynamic simulation of the flow in the bend. They modified this model by referring to the assumption of steady viscosity of vortices under standard conditions and hence inefficiency of this model in predicting sharply curved flows. Wu et al. [2] carried out a 3D investigation of flow pattern considering sediments as bed load and floating particles in a 180° bend. Kassem and Chaudhry [3] employed a 2D model to predict temporal bed-shifts in the bend. They also compared the results of modeling with experiment results, which indicated a desirable correspondence. Wilson et al. [4] also used SSIIM numerical model and studied flow pattern and colored matter stretching in a meandering laboratory channel. Wildhagen [5] used the numerical model of SSIIM to examine sediment transport in sharply bent channels. Aghaee and Hakimzadeh [6] conducted a simulation in RANS and LES software applications and reported that the RANS' results were more similar to experimental data,

✉ Chonoor Abdi Chooplou
a.chonoor@modares.ac.ir

Mohammad Vaghefi
Vaghefi@pgu.ac.ir

¹ Faculty of Civil and Environmental Engineering, Tarbiat Modares University, Tehran, Iran

² Department of Civil Engineering, Persian Gulf University, Bushehr 7516913817, Iran

underperforming only in demonstrating horseshoe vortices. Naji Abhari et al. [7] analyzed the flow pattern inside a 90-degree curve and studied flow rate and the Froude number with SSIIM. Then, they made a comparison of the model's results and the experimental data. Ghobadian and Mohammadi [8] incorporated SSIIM numerical model to predict flow fields in non-steady (convergent and divergent) river bends. Nekoufar and Kouhpari [9] modeled unsubmerged vanes upstream of bridge piers in a straight path in SSIIM 3D software. These vanes are installed as perpendicular to the flow. They found that this numerical model could be a good option for simulation of sediment transport and scour depth around bridge piers, and that non-submerged vanes resulted in reduction of the scour cavity around the pier. Abdallah Mohamed et al. [10] designed a three-dimensional numerical model to conduct simulations at bridge piers by applying SSIIM software. Akib et al. [11] utilized the numerical software of SSIIM2 to evaluate the amount of scouring and maximum scour depth around the bridge piers in the nature. Ehteram and Meymand [12] carried out a 3D simulation of flow and sediment patterns at the constriction made by a bridge with the help of SSIIM2 software. Bassar et al. [13] applied SSIIM for modeling a rectangular abutment. Ghobadian and Basiri [14] employed SSIIM 3D software to calculate local scour and sedimentation in a channel with a 60-degree bend. Azizi et al. [15] numerically analyzed the flow at a bridge pier with submerged vanes. Ouyang and Lin [16] examined varied shapes of vanes affecting scour at channel banks. They modeled the vanes of different shapes in varied rows, and also simulated the effect of boundary conditions and flow depth on bed topography. Johnson et al. [17], Parchami et al. [18], Vaghefi et al. [19], Zarei et al. [20] and Safaripour et al. [21] explored the influence of submerged vanes on scour at a laboratory bridge pier. They reported in the results that these vanes generally cause a decrease in scour around the bridge pier. Dey et al. [22] experimentally investigated the effects of the locations of different submerged vanes at a bend of 180°. As suggested in the results, implementation of vanes with a 15-degree horizontal angle leads to the best scour decrease at the outer bank. Karimi et al. [23] experimentally examined the effect of bridge piers inclination angle upon scour trend in a linear channel. A numerical model was developed by Hamidi and Siadatmousavi [24] for evaluating patterns of flow and scour around a pier by using SSIIM. Although they reached a successful numerical model of SSIIM for estimating scour depths in front of adjacent piers, they overvalued the depths between the piers. Vaghefi et al. [25] mathematically investigated the pattern of flow around a spur dike with a T shape by using SSIIM numerical model at attractive and repelling protective structures. Flow pattern and sediment transport were

studied by Khayyun and Mouhamed [26] a 4250-m-long river. They reported that SSIIM model is highly capable of evaluating and estimating water flow and bed sediment transport. Hammerling et al. [27] investigated distribution of velocity and alterations of bed topography at river bed by using SSIIM computer code. Asadollahi et al. [28] made a comparison of the data from experimental and numerical investigations on flow and scour patterns at single and triad bridge piers installed in a 180-degree sharp bend. Rasaei et al. [29] numerically modeled the scour cavity volume and maximum scour depth at piers located in a convergent river bend of 90° with a central radius of curvature equal to 1.7 m. The scour pattern at a convergent bend of 90° was efficiently simulated by the numerical model of SSIIM-2, which proved to have results well consistent with the experimental results. Asadollahi et al. [30] numerically and experimentally studied the scour and flow patterns with a set of piers located at different positions at a sharp bend of 180° and reported that positions of the piers at the bend had no impacts on the value and location of maximum scour depth. Ben Mohammad Khajeh and Vaghefi [31] examined the influences the abutments in the vicinity of a pier could have on the depth of scour in a sharp 180° bend. They detected in every test that the maximum scour depth happened upstream of the outer abutment. Moghanloo et al. [32] studied the collar level and thickness at an oblong pier with a bend of 180°, around which the scour cavity size was reduced. They reported that the collar thickness increase at the levels higher than the bed level raised the depth of scour. In addition, implementation of the collar in proximity of and under the initial bed level additionally decreased the scour cavity size at the pier in comparison with the pier accompanied by no collars. Sedighi et al. [33] did their investigations around convergent and divergent circular piers' scour for various angles of a 180° sharp bend experiencing varied flow regimes and concluded that the maximum scour depth was enhanced as they repositioned the convergent circular piers from the beginning bend of 90° to the ending bend of 90°. Abdi Chooplou et al. [34] numerically simulated the pattern of flow occurring around a pier with a single bridge upstream of submerged vanes affecting an alluvial bed in a sharp bend of 180°. Vaghefi et al. [35] numerically investigated variations of bed topography caused by placing a triad series of piers with a vertical bridge installed at a bend of 180° with varied relative radii by using the 3D numerical model of SSIIM. The studies conducted by Chauhan et al. [36] have provided valuable insights into the use of submerged vanes for sediment diversion. Their conclusions highlighted the current limitations in knowledge and suggested areas for future research in sediment diversion using submerged vanes. Sadeqlu and Hamidi [37] employed the numerical model of Flow-3D to

investigate the reduction of scour around a cylindrical bridge pier by installing a pair of submerged vanes in a straight path. Biswal and Das [38] utilized the SSIIM model to numerically simulate scour in two different flow field arrangements around piers. Harshvardhan and Kaushal [39] applied Computational Fluid Dynamics (CFD) to model local scouring around a bridge pier using the SSIIM numerical model. Abdi Chooplou et al. [40] conducted experimental investigations on the effects of submerged vanes with full overlapping length across the channel width on bed topography and scouring around a bridge pier in a sharp 180° bend. Their results demonstrated that the use of submerged vanes effectively reduced scouring. Majedi-Asl et al. [41] conducted experimental studies to evaluate the performance of submerged vanes, eppi, and sill in controlling scour depth around a group of bridge piers in a straight path. Fathi et al. [42] conducted experimental research to examine the effectiveness of riprap, submerged vanes, and their combination in reducing scour around vertical walls and spill-through abutments in a straight path. Niknezhad et al. [43] utilized the SSIIM2 model to investigate the impact of lateral intake positions on the flow pattern around a bridge pier with a 180° bend. Okhravi et al. [44] numerically modeled two groups of piles to evaluate local scouring in non-uniformly graded sediments using the SSIIM model. Sarlak et al. [45] conducted experimental investigations to study the effects of permeability and angle of gabion submerged vanes on bed topography.

So far, no comprehensive investigation of the effect of submerged vanes on the scouring of bridge piers, especially in a bend-shaped path, has been done numerically. Considering the expensive and time-consuming nature of experimental research, the need for numerical modeling and the use of existing software is evident. For this reason, in this research, the SSIIM numerical model was first investigated and validated in modeling the scour pattern in a sharp 180-degree bend combined with bridge piers and submerged vanes by using the experimental results of Abdi Chooplou et al. [40]. Since the length of overlapping vanes was constant and 100% in the research of Abdi Chooplou et al. [40], the changes in the position of the submerged vanes across the channel, as well as distances of the vanes from the center of the bridge pier and from each other with different 100, 50, and 0% overlapping lengths upstream of the pier, were investigated in this research after confirming the high ability of SSIIM numerical model for simulating scouring around the bridge pier with upstream submerged vanes in a sharp 180-degree bend. The numerical simulations of the bridge installed in a sharp 180-degree bend with a relative curvature equivalent to 2, changes in bed topography, longitudinal and transverse profiles of the bed, slope of the scour cavity wall around the pier in different

directions, maximum scour depth and percentage of its reduction, scour extension, length and width of the rectangle circumscribing the scour cavity at the pier, and area and volume of the scour cavity around the pier with their reduction percentages were comprehensively investigated.

Verification of the experimental model

Abdi Chooplou et al. [40] performed the experiments using a 180° curved channel located in the advanced hydraulics laboratory of the Persian Gulf University. This channel is comprised of a 6.5-m-long straight path upstream and a 5.1-m-long straight path downstream, linked with a 180° bend having an inner radius (R_i) of 1.5 m and an outer radius (R_o) of 2.5 m. This channel contains a sharp bend ($R_c/B < 3$) according to Leschziner and Rodi [46] classification. The channel is 0.7 m high and 1 m wide. The longitudinal slope of the bed equals 0.001 and is covered with sediments of averagely 1.5 mm diameter, standard deviation of 1.14 up to a depth of 30 cm. The inlet discharge capacity is 70 L per second under incipient motion conditions. The pier diameter (D) is 0.05 m. The submerged vanes employed in the experiments are Plexiglas with a length of 0.075 m, and a thickness of 0.01 m, submergence ratio for 75% at a 25-degree horizontal angle, and two positions, i.e., 40 and 60% of the width of the channel from the inner bank. The overlapping length of the vanes is equal to 100%. The submerged vanes installed at the upstream part of the pier are illustrated by Fig. 1.

This paper used SSIIM software, modeled a channel similar to the laboratory channel, and compared the bed topography in aforementioned parameters of the submerged vanes. L_{vb} denotes the distance from the vanes to the inner bank; L_{cv} shows the overlap length of the vanes; and L_{vp} and L_{vv} represent the distance of the vanes from the bridge pier and from each other, respectively.

Introduction of SSIIM numerical model and flow field equations

The ability of the SSIIM model to simulate sediment transport on mobile beds with complicated geometries is the main advantage compared to other CFD models. The Navier–Stokes relations of turbulent flows under an ordinary 3D geometry are solved in order to achieve water velocity. The turbulent shear stress can be calculated by using the k - ϵ model.

Equation of Navier–Stokes for modeling non-compressible flows with a constant density can be presented as follows:

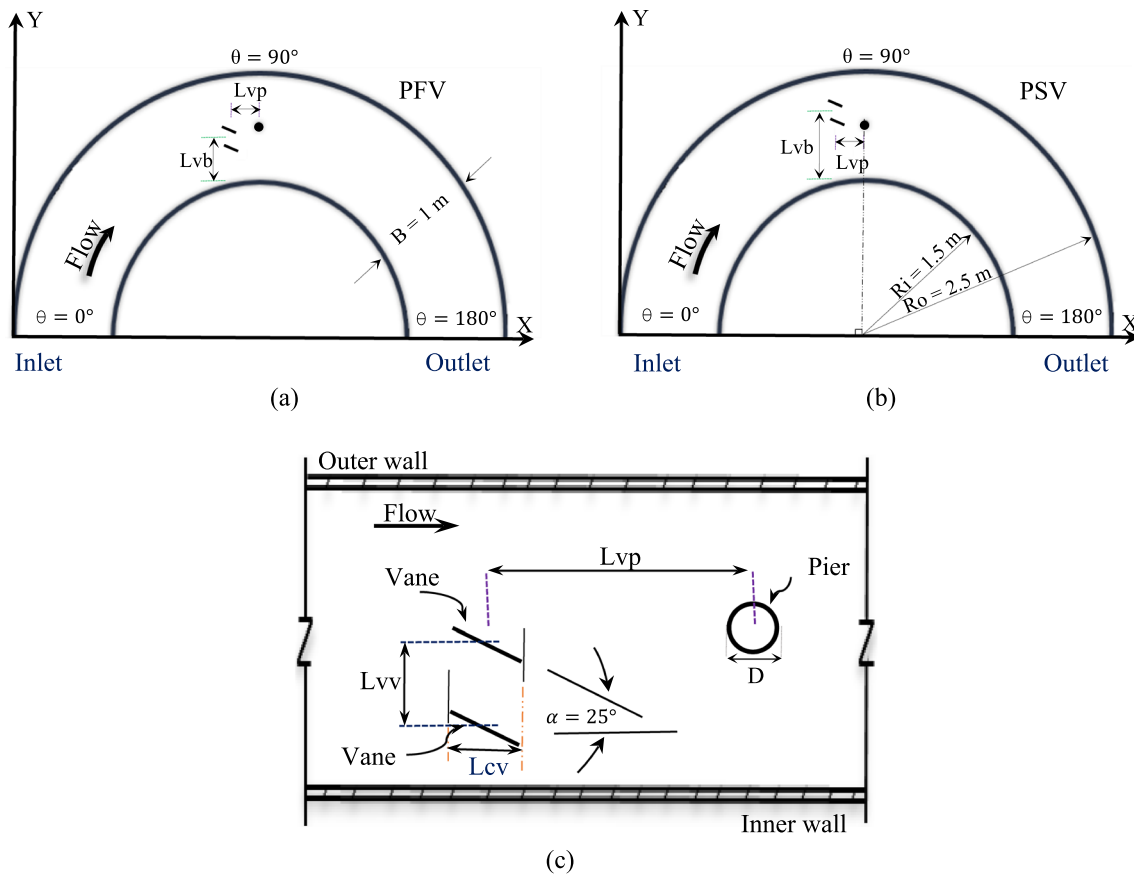


Fig. 1 A schematic view of installation of the submerged vanes at the upstream side of the bridge pier, where they were located at a distance of (a) 40 and (b) 60% of the channel width from the inner bank and (c) the symbols of pier and vanes

$$\frac{\partial U_i}{\partial t} + U_j \frac{\partial U_i}{\partial x_j} = \frac{1}{\rho_w} \frac{\partial}{\partial x_i} (-P\delta_{ij} - \rho \overline{u_i u_j}) \tag{1}$$

$$-\overline{u_i u_j} = \nu_T \left(\frac{\partial U_j}{\partial x_i} + \frac{\partial U_i}{\partial x_j} \right) + \frac{2}{3} k \delta_{ij} \tag{2}$$

Here x represents distance, U is velocity in three directions, P denotes total pressure, and δ_{ij} is the Kronecker delta that is unity if $i=j$, and equals 0 if not [47].

The first and second terms on the left side refer to local and convective accelerations, respectively.

On the right hand, the terms, respectively, denote pressure and the Reynolds stress. Evaluation of this term requires a turbulence model.

A control-volume method can be used to discretize the equations. Furthermore, the multi-block option can be dealt with by using an implicit solver. The pressure can be corrected by default via the SIMPLE method. The power-law and second-order upwind schemes are applied to discretize the convective terms [47].

The term of Reynolds stress is modeled by introducing the eddy-viscosity concept together with the Boussinesq approximation with the help of Eq. (2):

According to the Navier–Stokes equation, the diffusive term is shown via the first right-hand term, while the second term is usually ignored. The third term, which is trivial and normally insignificant, is used for the pressure [47].

In this study, the $k-\epsilon$ turbulence model was selected for better predictions of turbulent vortices and scouring according to the recommendations of various researchers [7–9, 14, 15, 24, 34, 35]. By using Eq. (3), the eddy-viscosity concept is calculated based on the $k-\epsilon$ model:

$$\nu_T = c_\mu \frac{k}{\epsilon} \tag{3}$$

represents The turbulent kinetic energy is depicted by $k-\epsilon$ modeled via Eq. (4):

$$\frac{\partial k}{\partial t} + U_j \frac{\partial k}{\partial x_j} = \frac{\partial}{\partial x_j} \left(\frac{\nu_T}{\sigma_k} \frac{\partial k}{\partial x_j} \right) + P_k - \epsilon \tag{4}$$

Here, P_k is obtained through Eq. (5):

$$P_k = \nu_T \frac{\partial U_j}{\partial x_i} \left(\frac{\partial U_j}{\partial x_i} + \frac{\partial U_i}{\partial x_j} \right) \tag{5}$$

ϵ represents dissipation of k , which is modeled as follows:

$$\frac{\partial \epsilon}{\partial t} + U_j \frac{\partial \epsilon}{\partial x_j} = \frac{\partial}{\partial x_j} \left(\frac{\nu_T}{\sigma_\epsilon} \frac{\partial \epsilon}{\partial x_j} \right) + C_{\delta 1} \frac{\epsilon}{K} P_k + C_{\delta 2} \frac{\epsilon^2}{K} \tag{6}$$

where the constant values for k - ϵ model are stated below and the user is unable to change them [29]:

$$c_\mu = 0.09 \quad C_{\epsilon 1} = 1.44 \quad C_{\epsilon 2} = 1.92 \quad \sigma_\epsilon = 1.3$$

For a suspended load near bed, a formula was proposed by Van Rijn [48] to calculate concentration of the equilibrium sediment, C_{bed} :

$$C_{bed} = 0.015 \frac{d_{50}^{0.3}}{a} \frac{\left[\frac{\tau - \tau_c}{\tau_c} \right]^{1.5}}{\left[\frac{(\rho_s - \rho_w)g}{\rho_w v^2} \right]^{0.1}} \tag{7}$$

where d_{50} is the particle diameter of the sediment; a shows a set of the reference levels corresponding to roughness height; τ denotes bed shear stress; τ_c stands for the critical shear stress of the bed based on the motion of sediment particles maintained by the shields curve; ρ_w and ρ_s demonstrate water and sediment densities, respectively; ν represents water viscosity (m^2/s); and g is acceleration of gravity [47].

The bed load shown by q_b can be obtained besides the suspended load. Equation (8) helps calculation of bed load via Van Rijns formula [48]:

$$\frac{q_b}{d_{50}^{1.5} \sqrt{\frac{(\rho_s - \rho_w)g}{\rho_w}}} = 0.053 \frac{\left[\frac{\tau - \tau_c}{\tau_c} \right]^{2.1}}{d_{50}^{0.3} \left[\frac{(\rho_s - \rho_w)g}{\rho_w v^2} \right]^{0.1}} \tag{8}$$

where a stands for base surface, which is equivalent to roughness height; τ denotes shear stress of the bed; and τ_c represents critical shear stress for particles incipiently moving on the bed [48]. The SSIIM numerical model uses several files to perform calculations and present results. All these files are of ASCII type. The two main input files of the program are Control and Koordina. The file of Koordina represents geometrical coordinates of the mesh and the file of Control contains other input parameters. In the simulation used in this research, a fixed flow discharge of $0.07 \text{ m}^3/s$ and a fixed upstream depth of 0.18 m were applied in the Control input file. The flow depth was selected in such a way that the flow conditions were considered to be close to the movement threshold based on the constant input flow discharge (Neill [49]; De Medeiros et al. [50]). The bridge pier with a diameter of 5 cm was considered in the model according to the recommendations of Chiew and Melville [51] and Amini and Mohammad [52]. Two vanes with a length of $1.5D$ and a thickness of $0.2D$ with 75% submersion, an angle of 25° compared to the horizon line (Odgaard and Wang [53]) in different positions in the channel width and length, and varied overlapping lengths of 100, 50, and 0% according to Fig. 2 were simulated in the SSIIM software. According to the recommendations of Raudkivi and Ettema [54] and Raudkivi [55], the size of sediment particles was regarded to be 0.0015 m in the simulated model. The velocity of the falling sediment particles was chosen as 0.011 m/s . The sediment density and Shields coefficient of critical bed shear stress for movement of the sediment particles were introduced as 2650 kg/m^3 and 0.028 in the model, respectively.

Various meshes of different sizes were created and implemented in the models to determine the optimal one. The results indicated that while the uniform mesh with a small size provided high accuracy and closely matched the laboratory values of bed topography changes, it

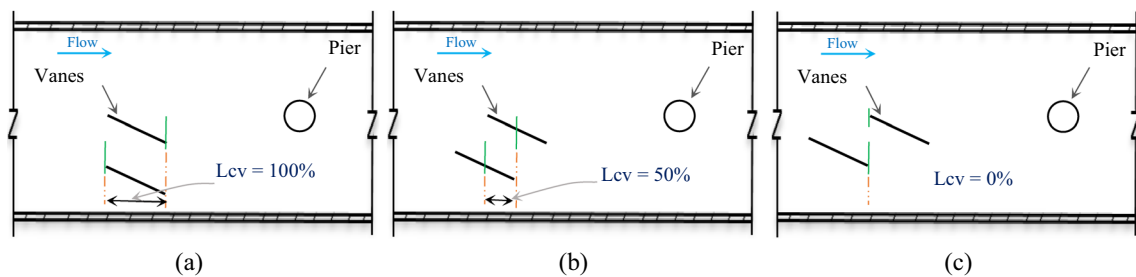


Fig. 2 A schematic view of the submerged vanes at the upstream part of the bridge pier with variable overlapping lengths of **a** 100%, **b** 50%, and **c** 0%

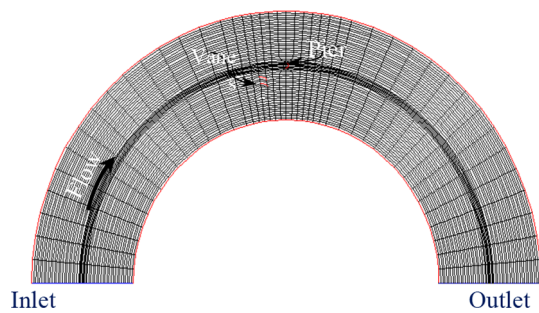


Fig. 3 A view of the mesh points

increased the running time. As a result, a non-uniform meshing approach was employed with smaller cells around the bridge pier and submerged vanes. 45 and 55 sections were, respectively, utilized in the longitudinal and transverse directions as shown in Fig. 3.

To define the boundaries in the numerical SSIIM software, all boundaries, including the bridge pier and submerged vanes, were set as rigid boundaries by introducing the relevant parameters in the program’s control menu. In this study, the boundaries around the bridge pier and vanes were defined as rigid to ensure that the flow lines passed through them without any collision. It is worth noting that all

Fig. 4 Example of the comparison between numerical and experimental models regarding the bed lateral profile at a distance of 3D toward upstream of the pier with vanes placed at a distance of **a** 0.4B and **b** 0.6B from the inner bank

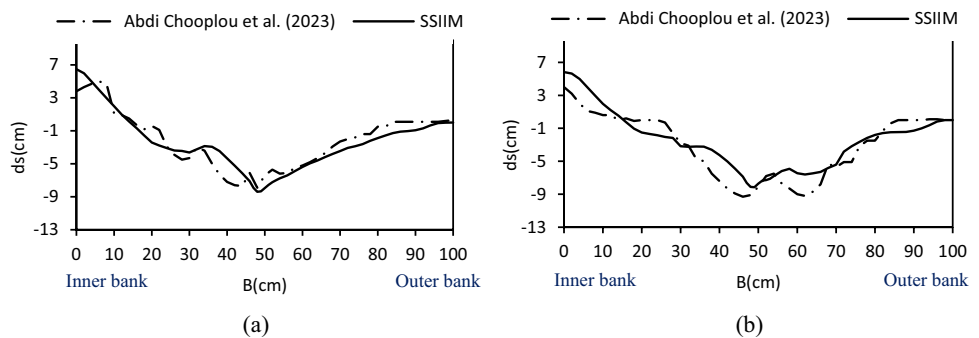


Fig. 5 An instance of the numerical and experimental comparison of the bed lateral profile at the location of the pier with vanes installed at a distance of **a** 0.4B and **b** 0.6B from the inner bank

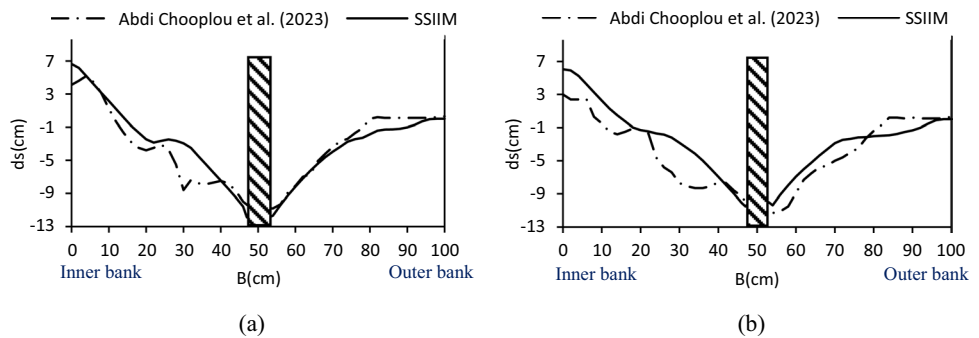
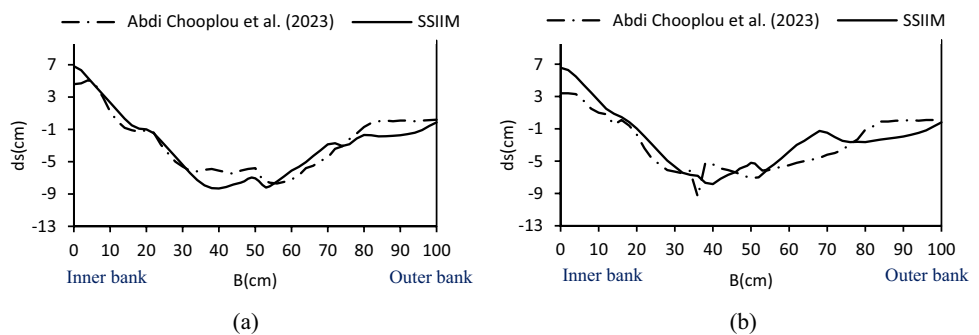


Fig. 6 An instance of the numerical and experimental comparison of the bed lateral profile at a distance of 3D toward the downstream side of the pier with vanes installed at a distance of **a** 0.4B and **b** 0.6B from the inner bank



runs were conducted on a standard computer equipped with a Cori 5 processor running at a speed of 2000 MHz. Implementation of the sedimentation took approximately 24 h. Additionally, in the software, the equations were converged by setting the remaining numerical calculations, velocity parameters in the longitudinal, transverse, and depth directions, and continuity equations to zero using the $k-\epsilon$ method. Furthermore, the equations for kinetic energy and its loss were accepted when they converged and approached zero with an accuracy criterion of 10^{-4} for analysis.

Validation of the numerical models

Figures 4, 5, 6 illustrate instances of bed cross-sectional topography at the upstream and downstream sides of the bridge for both numerical and experimental models. The channel width has been denoted by B , and bed level by ds . Sedimentation has occurred at the inner bank at a distance 3 times the pier diameter toward the upstream side of the pier in both models (Fig. 4).

At sections crossing the bridge pier location (Fig. 5), SSIIM numerical model has accurately simulated the experimental model. Therefore, in both of the models, sedimentation happens at the channel inlet in the vicinity of the inner

bank, and the maximum scour is found at the pier. From the maximum scour location to $0.8B$ away from the inner bank, the scour is lessened and has trivial variations up to the outer bank.

As shown in Fig. 6, both experimental and numerical models indicate an appropriate correspondence between bed alterations and maximum scours. This is indicative of high capability of this numerical model in determination of scour pattern in curved channels containing hydraulic structures such as bridge piers and submerged vanes.

Figure 7 depicts a point-by-point comparison of bed levels in the numerical and experimental models with vane installation at the distances of 40 and 60% of the width of the channel from the inner bank. It may be observed from the segment bisector that the values of the experimental and numerical models are similar, and generally fall at a range of 20% error, where the highest bed level difference between the two models occurs along the last third of the bend.

The mean absolute error (MAE) and the root mean squared error (RMSE) were incorporated in this paper to address the SSIIM numerical model error relative experimental models' error. The relations below help obtain MAE and RMSE [56]:

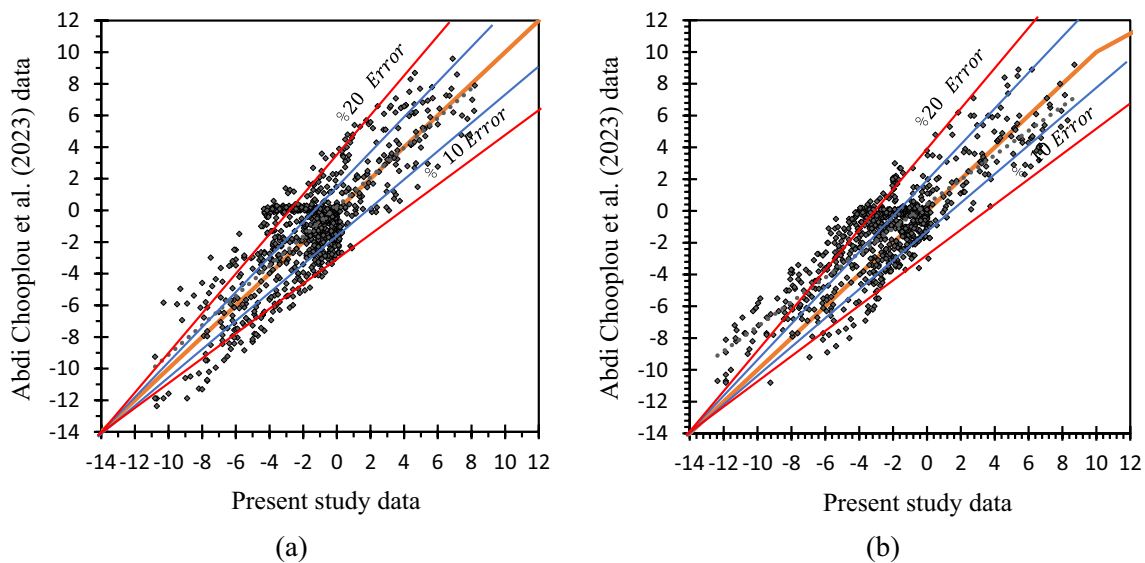


Fig. 7 Comparison of bed topography data of the numerical and experimental models with vanes installed at a distance of **a** 0.4B and **b** 0.6B from the inner bank

Table 1 Errors of SSIIM numerical model in the simulation

Row	Symbol of run	Lvb/B	Lcv, (%)	Lvp/D	MAE	RMSE
1	PFV	0.4	100	5	0.014	0.018
2	PSV	0.6	100	5	0.015	0.019

$$\text{MAE} = \frac{\sum_{i=1}^N |y_{\text{Lap}} - y_{\text{SSIIM}}|}{N} \quad (9)$$

$$\text{RMSE} = \sqrt{\frac{\sum_{i=1}^N (y_{\text{Lap}} - y_{\text{SSIIM}})^2}{N}} \quad (10)$$

In the relations above, (y_{Lab}) and (y_{SSIIM}) are the values obtained from the bed topography in the laboratory by Abdi Chooplou et al. [40] and the numerical model, and N denotes the total number of data.

Given the values obtained through Eqs. (9) and (10) for validations made in Table 1, it may be concluded that the numerical model of SSIIM can accurately simulate scour pattern in the 180° sharp bend with a pier and submerged vanes.

After confirming the numerical model, the authors simulated the 100% overlapping lengths of RMSE and MAE in the ranges of 0.0180–0.024 and 0.016–0.019, respectively, in order to comprehensively examine the different overlapping lengths according to the series of experiments conducted by Abdi Chooplou et al. [40].

Research limitations

In general, in the SSIIM software, the mesh lines in the vertical direction must be exactly straight and the piers and vanes must have a perpendicular geometry. In this research, the limitations of the flow hydraulic conditions included the inlet discharge and the upstream flow depth, which was considered constant. The grading of materials and geometries of the bridge piers and submerged vanes were also considered to be fixed.

Results and discussion

The first stage involved examination of the single bridge pier model to compare the results on the effect of using submerged vanes upstream of the bridge pier with those of the model with no vanes placed upstream of piers. 54 models were then developed by placing 2 submerged vanes upstream of the bridge pier. The models' characteristics and symbols and the results on the function of vanes in decreasing the maximum scour and sedimentation are presented in Table 2. The bridge pier and the submerged vane are denoted by, respectively, P and V. The vanes' positions at channel width and at a distance of 0.4B and 0.6B from the inner bank are, respectively, represented by F and S. Table 2 indicates that the maximum scour depth (d_{smax}) and the maximum sedimentation height (h_{max}) in the single bridge pier model

with no upstream submerged vanes (P), respectively, occur for 2.68D and 1.96D. The presence of The scour depth has been reduced around the bridge pier by the submerged vanes at its upstream part. Installation of the submerged vanes at the distance of 0.4B from the inner bank has led to the lowest (15.67%) and highest (50.60%) reductions of maximum scour depth in the models of PFV7 and PFV12, respectively. In addition, their installation at the distance of 0.6B from the inner bank has resulted in the lowest (18.68%) and highest (28.28%) reductions of maximum scour depth in the models of PSV20 and PSV8, respectively. Generally, the maximum scour depth decreased by approximately 27%. Safaripour et al. [21] also fixed the position of the vanes in the middle of the channel width (0.5B) with the distances of 0.125 and 0.075 m from the bridge pier and from each other, respectively, and an angle of 25° with 100% overlapping of vanes. By changing the submergence ratio of the vanes, they concluded that the reductions in the maximum scour depth in the single-pier and triad-pier tests were nearly 30 and 23% in comparison to the test with no submerged vanes installed, respectively. Given the percentage of reduction in the maximum sedimentation in comparison with the single-pier model in Table 2, it may be observed that reductions in the maximum sedimentation in models with presence of submerged vanes at the distance of 0.4B from the inner bank are in the range of 6.53–14.3%. The highest reduction in sedimentation in comparison with the model of the bridge pier with no submerged vanes installed occurs in PFV22. Moreover, with installation of the submerged vanes 60% of the channel width away from the inner bank, the highest and the lowest contribution of the vanes to reduction of the maximum sedimentation height occur, respectively, in PSV25 and PSV18 models, which correspondingly result in 20.41 and 14.68% reductions in sedimentation height compared to the single-pier model.

Figure 8 shows an example of alterations in bed topography leading to the lowest and highest reductions of maximum scour depth in the studied models. It may be observed that the scour cavity appearing around the pier has been caused by vortices occurring around it, and the main scour cavity has no symmetry relative to the channel's longitudinal axis. Such an asymmetry occurs owing to the presence of the pier inside the sharp bend. Further, the scour cavity is comprised of two parts, one approaching the outer bank with less skewedness toward downstream, and the other skewed in the inner bank direction because of the vortices composition around the pier and the helical flow. The vanes' arrangement at 0.4B from the inner bank makes the sediments between the vanes orient toward the scour cavity at the bridge pier. As a result, the scour depth occurring at the proximity of the pier in PFV12 in Fig. 8a undergoes a considerable decrease and the smallest scour depth value of all takes place in this arrangement. Even though the maximum

Table 2 Properties and results of different models

Run No.	Symbol of run	Lvb/B	Lev, (%)	Lvp/D	Lvv/D	dsmax/D	Reduction of dsmax, (%)	hmax/D	Reduction of hmax, (%)
1	P	–	–	–	–	2.68	–	1.96	–
2	PFV1	0.4	100	2.5	1	1.58	41.04	1.71	12.55
3	PFV2	0.4	100	2.5	1.5	1.72	35.82	1.83	6.53
4	PFV3	0.4	100	2.5	2	1.44	46.27	1.81	7.55
5	PFV4	0.4	100	5	1	2.14	20.15	1.70	13.27
6	PFV5	0.4	100	5	1.5	1.40	47.76	1.80	8.16
7	PFV6	0.4	100	5	2	2.16	19.40	1.72	12.24
8	PFV7	0.4	100	7.5	1	2.26	15.67	1.72	12.24
9	PFV8	0.4	100	7.5	1.5	2.24	16.42	1.72	12.24
10	PFV9	0.4	100	7.5	2	1.61	39.93	1.76	10.20
11	PFV10	0.4	50	2.5	1	1.56	41.79	1.75	10.61
12	PFV11	0.4	50	2.5	1.5	1.82	32.09	1.74	11.02
13	PFV12	0.4	50	2.5	2	1.32	50.60	1.76	10.20
14	PFV13	0.4	50	5	1	2.14	20.15	1.73	11.63
15	PFV14	0.4	50	5	1.5	1.50	44.03	1.76	10.20
16	PFV15	0.4	50	5	2	2.04	23.88	1.78	9.18
17	PFV16	0.4	50	7.5	1	2.24	16.42	1.72	12.24
18	PFV17	0.4	50	7.5	1.5	2.24	16.42	1.76	10.20
19	PFV18	0.4	50	7.5	2	2.11	21.12	1.76	10.00
20	PFV19	0.4	0	2.5	1	1.48	44.78	1.70	13.27
21	PFV20	0.4	0	2.5	1.5	1.38	48.51	1.76	10.20
22	PFV21	0.4	0	2.5	2	1.41	47.31	1.76	10.20
23	PFV22	0.4	0	5	1	2.18	18.66	1.68	14.29
24	PFV23	0.4	0	5	1.5	1.50	44.03	1.78	9.18
25	PFV24	0.4	0	5	2	2.06	23.13	1.70	13.37
26	PFV25	0.4	0	7.5	1	2.24	16.42	1.70	13.27
27	PFV26	0.4	0	7.5	1.5	1.98	26.12	1.72	12.24
28	PFV27	0.4	0	7.5	2	2.18	18.66	1.74	11.22
29	PSV1	0.6	100	2.5	1	2.14	20.15	1.65	16.02
30	PSV2	0.6	100	2.5	1.5	2.10	21.64	1.61	18.06
31	PSV3	0.6	100	2.5	2	2.11	21.34	1.60	18.57
32	PSV4	0.6	100	5	1	2.07	22.84	1.64	16.33
33	PSV5	0.6	100	5	1.5	2.08	22.54	1.66	15.51
34	PSV6	0.6	100	5	2	2.10	21.57	1.58	19.39
35	PSV7	0.6	100	7.5	1	1.95	27.24	1.64	16.43
36	PSV8	0.6	100	7.5	1.5	1.92	28.28	1.64	16.22
37	PSV9	0.6	100	7.5	2	1.99	25.82	1.66	15.10
38	PSV10	0.6	50	2.5	1	2.08	22.24	1.61	17.96
39	PSV11	0.6	50	2.5	1.5	2.10	21.57	1.56	20.20
40	PSV12	0.6	50	2.5	2	2.12	21.06	1.60	18.47
41	PSV13	0.6	50	5	1	2.07	22.91	1.65	15.65
42	PSV14	0.6	50	5	1.5	2.09	22.15	1.64	16.38
43	PSV15	0.6	50	5	2	2.08	22.31	1.58	19.29
44	PSV16	0.6	50	7.5	1	1.97	26.49	1.66	15.12
45	PSV17	0.6	50	7.5	1.5	1.98	26.27	1.66	15.11
46	PSV18	0.6	50	7.5	2	1.94	27.61	1.67	14.67
47	PSV19	0.6	0	2.5	1	2.08	22.39	1.66	15.31
48	PSV20	0.6	0	2.5	1.5	2.18	18.66	1.58	19.39
49	PSV21	0.6	0	2.5	2	2.09	22.01	1.64	16.33

Table 2 (continued)

Run No.	Symbol of run	Lvb/B	Lcv, (%)	Lvp/D	Lvv/D	dsmax/D	Reduction of dsmax, (%)	hmax/D	Reduction of hmax, (%)
50	PSV22	0.6	0	5	1	2.11	21.42	1.64	16.33
51	PSV23	0.6	0	5	1.5	2.13	20.67	1.61	17.86
52	PSV24	0.6	0	5	2	2.11	21.27	1.61	17.65
53	PSV25	0.6	0	7.5	1	1.96	26.94	1.56	20.41
54	PSV26	0.6	0	7.5	1.5	2.00	25.37	1.60	18.37
55	PSV27	0.6	0	7.5	2	2.03	24.09	1.59	18.67

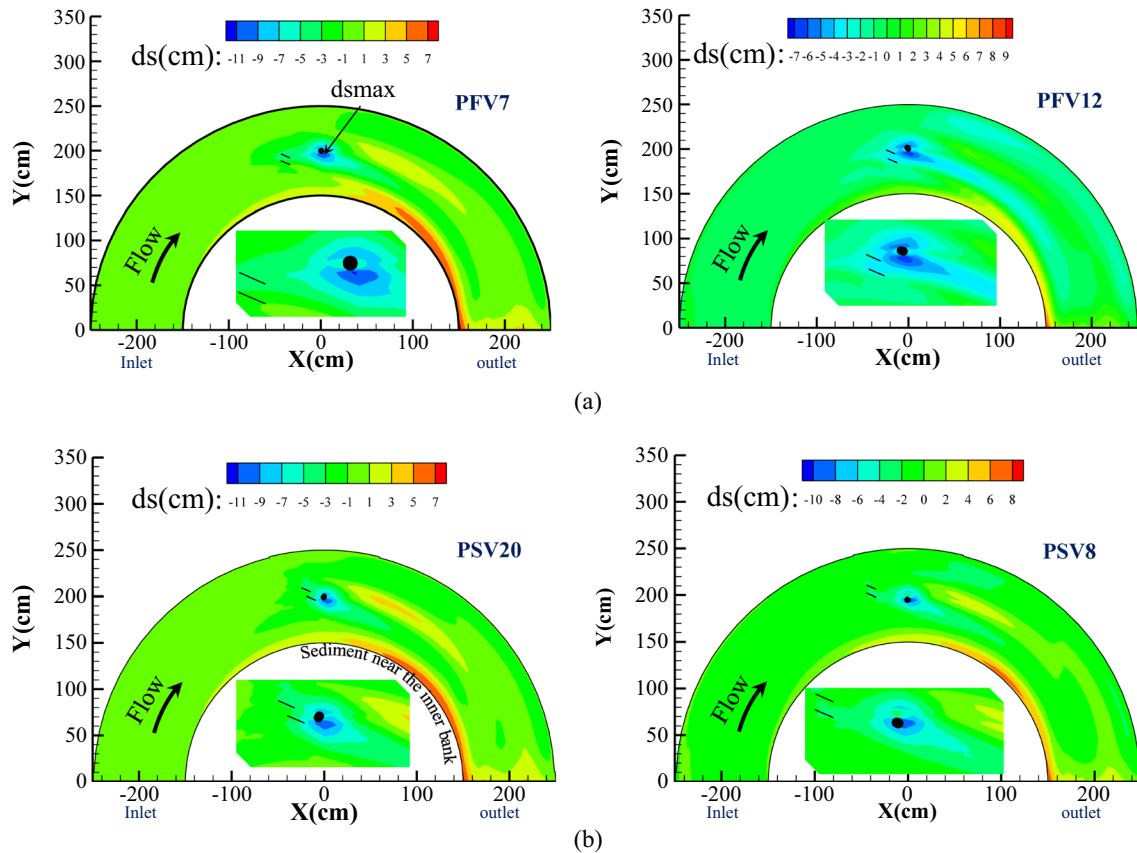
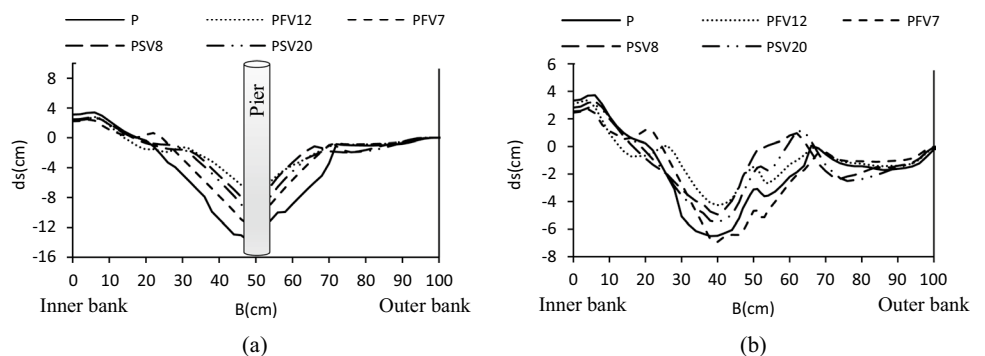


Fig. 8 An instance of the bed topography of the highest and the lowest maximum scours with vanes installed at a distance of **a** 0.4B and **b** 0.6B from the inner bank

Fig. 9 An instance of cross sections at (a) the pier location and (b) a distance of 4D from the pier location in downstream direction in models with the highest and the lowest maximum scours



scour depth in PFV7 is greater than that of PFV12, the scour cavity created at the pier toward downstream in PFV12 is nearly twice as large as that in PFV7. With the submerged vanes located at a distance of 60% the channel width from the inner bank shown in Fig. 8b, the scour depth has a direct relation with the scour cavity. Hence, the maximum degree of this skewing is observed in PSV20, one which expands over a distance of 20D toward downstream.

The cross section shown at the pier location (Fig. 9a) refers to contribution of the performance of submerged vanes to scour reduction around the pier. The scour cavity has expanded from a distance of 15 to 75% of the channel width from the inner bank in different models, and in the case of a single pier, increase in depth and further expansion of the scour cavity are observed. The scour cavity depth has averagely lowered by 50% as the vanes were installed. In PFV12 model, the lowest amount of scour at this section as well as the sections in the vicinity indicates the contribution of the submerged vane to scour reduction. This trend is also observed at downstream sections, an instance of which is shown in Fig. 9b for the cross section at a distance of 4D toward the downstream side of the pier. Also, the flow of

water carries the sediments collected from the areas around the pier and the submerged vanes with it, and considering this section, some of these sediments have been accumulated at the inner bank at downstream sections; the highest accumulation occurs in P model with a value of 0.8 times the pier diameter, equal to 4 cm at a distance of 6% of the channel width from the inner bank. With presence of the vanes in every model except PVF7 model, the amount of scour has significantly decreased at a range of 25–65% of the channel width from the inner bank.

Figure 10 is the illustration of an instance of bed topography changes in models having the greatest and the smallest maximum sedimentation heights. Sedimentation occurs due to formation of down flows near the pier and vortices moving from the upstream side in downstream direction, transporting a part of the washed bed materials toward downstream, and also because of the direction of near-bed lateral flows toward the inner bank, sediment piles have been formed in the vicinity of this wall. As seen in Fig. 10a, given the bed topography in the two selected models when the installed vanes are located 0.4B from the inner bank, it may be observed that a decrease of 20% in maximum scour depth

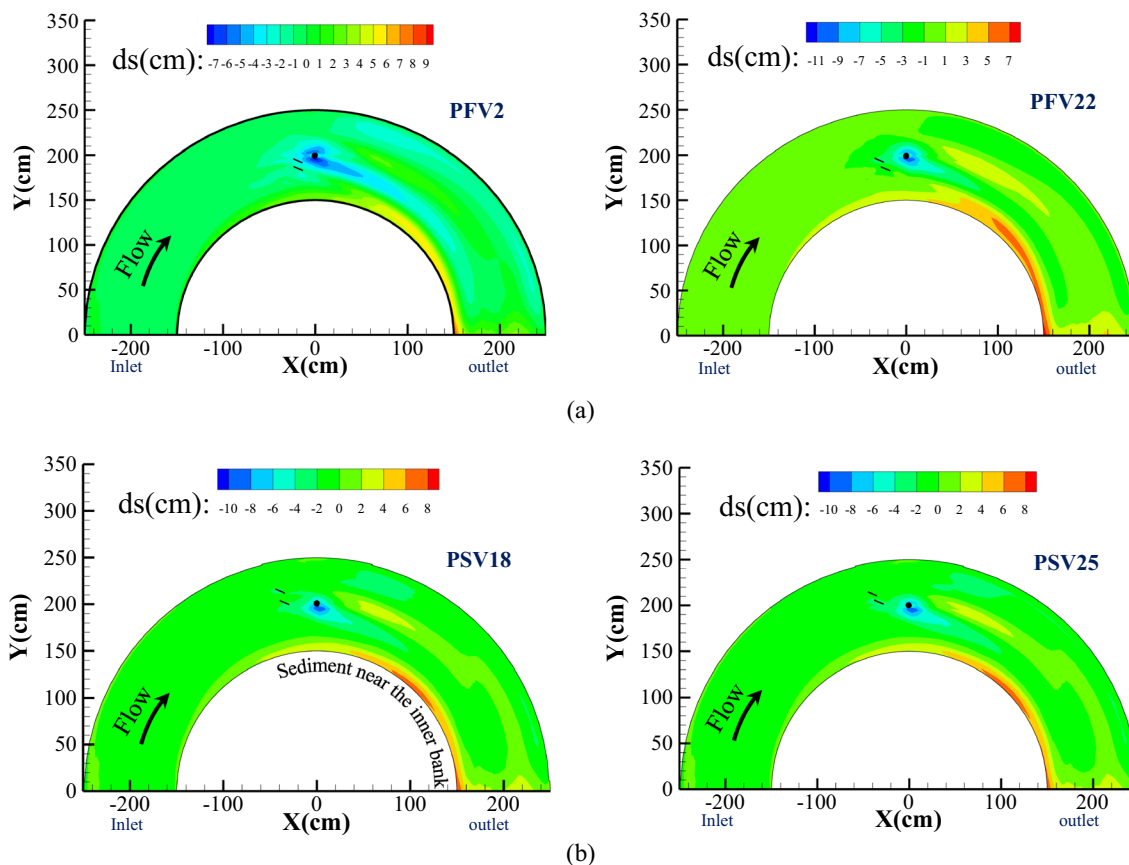


Fig. 10 Example of bed topography for the greatest and the smallest maximum sedimentation heights with vanes installed at a distance of **a** 0.4B and **b** 0.6B from the inner bank

Fig. 11 An instance of the longitudinal section, nondimensionalized with the pier diameter, at a distance of **a** 5 and **b** 50% of the channel width from the inner bank in models with the highest and the lowest sedimentations

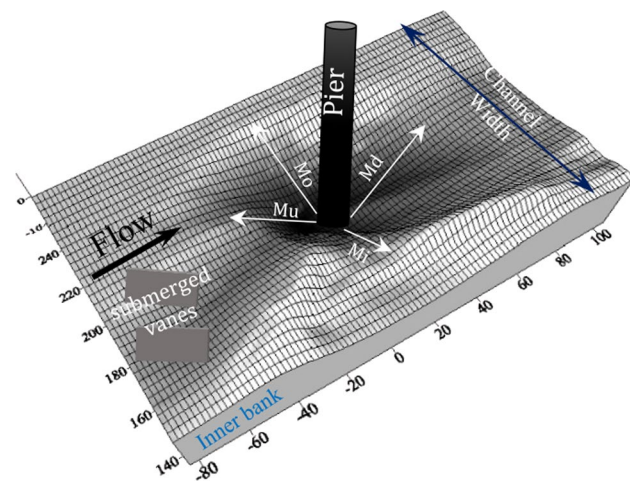
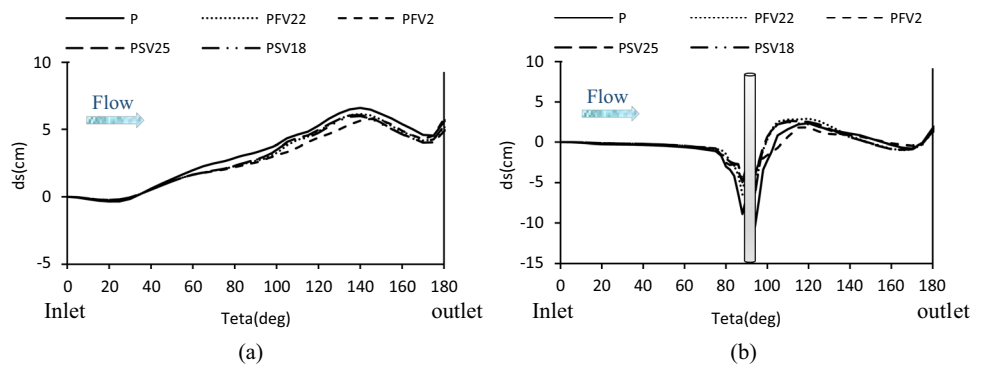


Fig. 12 Schematic view of the slope of the wall of the scour cavity around the pier

results in an increase of 9% in the maximum sedimentation height. This is caused by the combination of the impacts of the submerged vanes, pier, and bend on the flow pattern. As represented in Fig. 10b, the decrease and increase of 0.6 and 7% in the maximum sedimentation height and scour depth are seen when the vanes are installed at the distance of 0.6 B from the inner bank.

Figure 11 depicts an instance of longitudinal sections near the inner bank and the middle of the bend in models with the highest and the lowest maximum sedimentation heights. It may be observed in Fig. 11a that a trivial scour has occurred in every model near the inner bank, where the maximum scour depth of $0.06D$ is observed in P model in the 20° angle from the bend entrance. The sedimentation governs from about the position of 25° up to the end of the bend, which is more evidently represented in the second half part since the output sediments of the scour cavity are on a path line falling at the maximum velocity's geometric location in the bend, which entails sediment diversion toward the inner bank. Thenceforth, crossing this pile, the flow hits the bed at a higher velocity, digging sediments from those regions.

With submerged vanes implemented from the 58° position to the end of the bend, less sediment accumulation occurs compared to the single-pier model. This is indicative of the fact that a higher amount of sediments is directed toward the cavity around the pier in the presence of the submerged vanes compared to when they are absent. According to Fig. 11b, at 50% of the longitudinal section of the width of the channel from the inner bank, from the bend entrance up to the 32° angle, the bed does not undergo any significant alterations, and the trend of scouring in the models is similar up to the 70° angle. As expected, the maximum scour has occurred at the apex and the location of the pier. Since the return flows are more powerful in the single-pier model, the depth of this scour is much more in this model, and it is significantly reduced with installation of the vanes.

The scour cavity is enlarged with an inconstant slope in different directions. Figure 12 presents a schematic illustration of the scour cavity slope. μ_u , μ_d , μ_i , and μ_o here, respectively, refer to the slope in the upstream and downstream directions, as well as the inner and outer bank directions. The values of slopes in every model are shown in Fig. 13. The slopes in upstream, downstream, inner bank, and outer bank directions were measured in P model as, respectively, 0.48, 0.18, 0.36 and 0.38. In every executed model, the upstream slope was sharper than the downstream slope, and in the single pier, the slope of the scour cavity around the pier in upstream direction is approximately twice that in downstream direction. As is observed in Fig. 13a, the upstream and downstream slopes have been reduced by the submerged vanes upstream of the bridge pier. The maximum downstream slope has occurred in the presence of submerged vanes in PFV15 model, and the minimum in PFV6 arrangement. With values of the inner and the outer bank slopes taken into consideration, it may be observed that PFV17 and PFV7 models have the mildest slopes among all the models. A comparison between the scour cavity slopes around the pier in PFV3 indicates that all the slopes in this model are approximately equal, and the scour cavity around it is bowl-shaped. It may be reasoned that the bend effect is lower with arrangement of submerged vanes with 100%

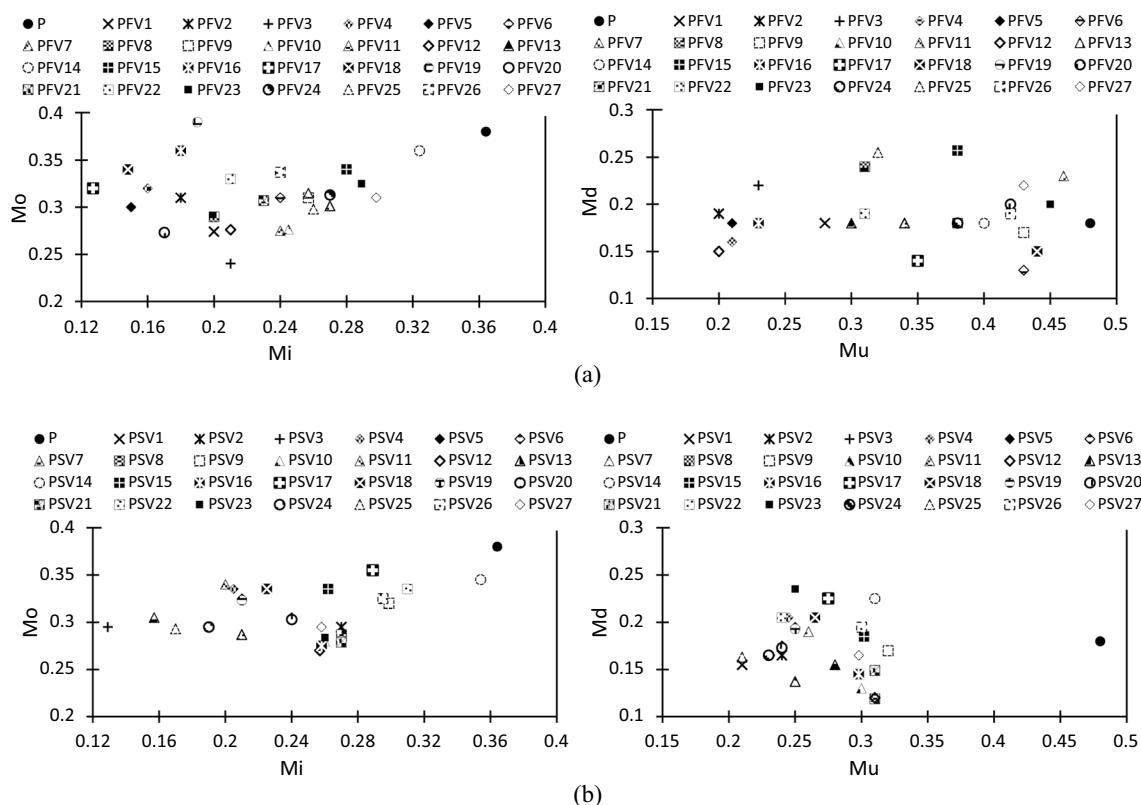


Fig. 13 The slope of the wall of the scour cavity around the pier with vanes installed at a distance of a 0.4B and b 0.6B from the inner bank

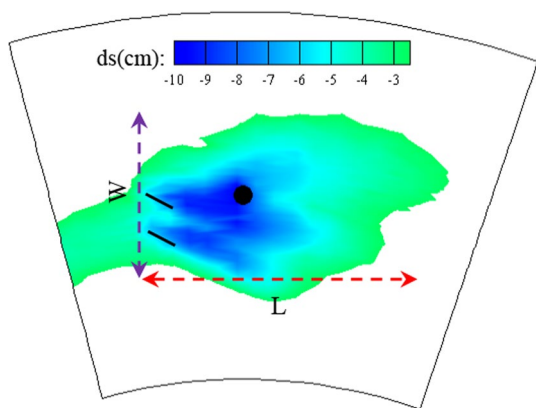


Fig. 14 Schematic illustration of the rectangle circumscribing the scour cavity at the pier

overlap with 2.5D and 2D distances, respectively, between the vanes and the piers and between the vanes themselves. As is observed in Fig. 13b, the presence of submerged vanes has resulted in the difference of the scour cavity slope is less visible relative to the channel’s longitudinal axis. Therefore, the scour cavity slopes in inner bank and outer bank directions in PSV14 model are equal. The presence of the submerged vanes has led to a milder scour cavity than the

lateral axis of the channel. Furthermore, in PSV9 model, the slope of the scour cavity in the direction of the lateral axis of the channel is symmetric. The cavity around the pier in that model has developed in upstream and downstream directions with the same slope. The maximum inner bank and outer bank slopes have been developed by the submerged vanes in PSV14, and the minimum slopes, respectively, in PSV3 and PSV12.

To demonstrate the scour cavity reach around the pier in length and width of the channel, a rectangle is circumscribed over this cavity. The scour cavity is represented by the scour depth, which is more than 50% of the pier diameter has been considered as. A schematic view of this rectangular shape is depicted in Fig. 14.

Figure 15 depicts length and width values of the circumscribed rectangle. It may be observed that for every model, the dimensions of the circumscribed rectangle are smaller than that in the bridge pier model with no submerged vanes present at the upstream side. In the model containing no upstream submerged vanes, these dimensions are, respectively, 21D and 7.5D. In PFV20, the length of the rectangle is much larger than its width, which is indicative of the fact that in this case, the sediment reach is much more in the longitudinal compared to lateral axis of the channel. It is also evident that the effect of changes in the length of

Fig. 15 Size of the circumscribing rectangle, dimensionless with the pier diameter, over the scour cavity at the pier with vanes placed at a distance of **a** 0.4B and **b** 0.6B from the inner bank

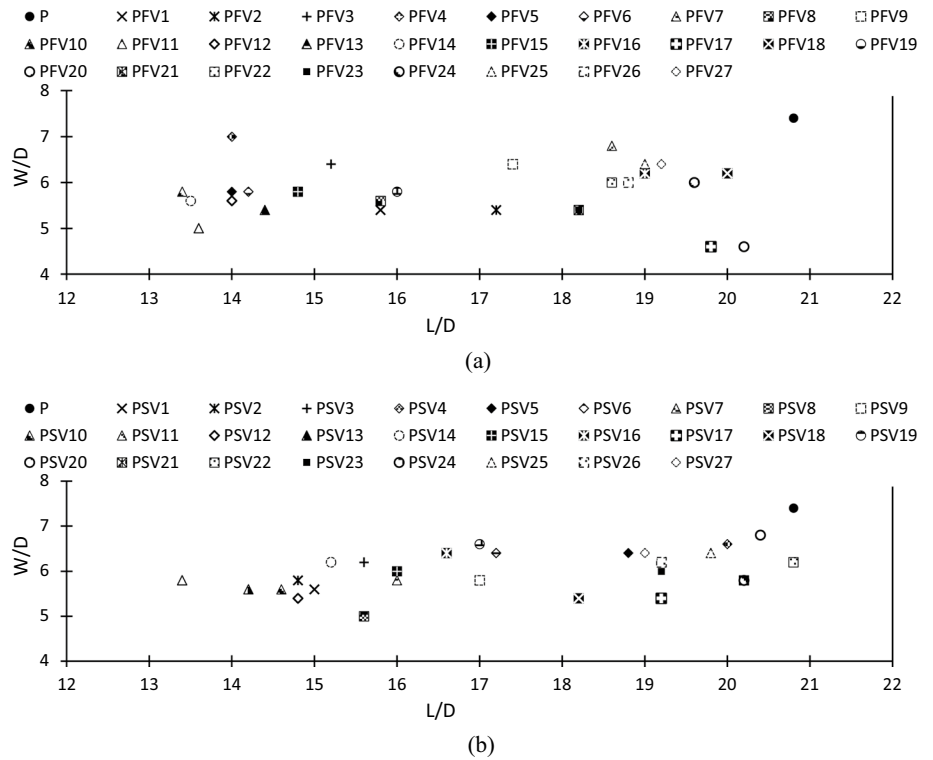
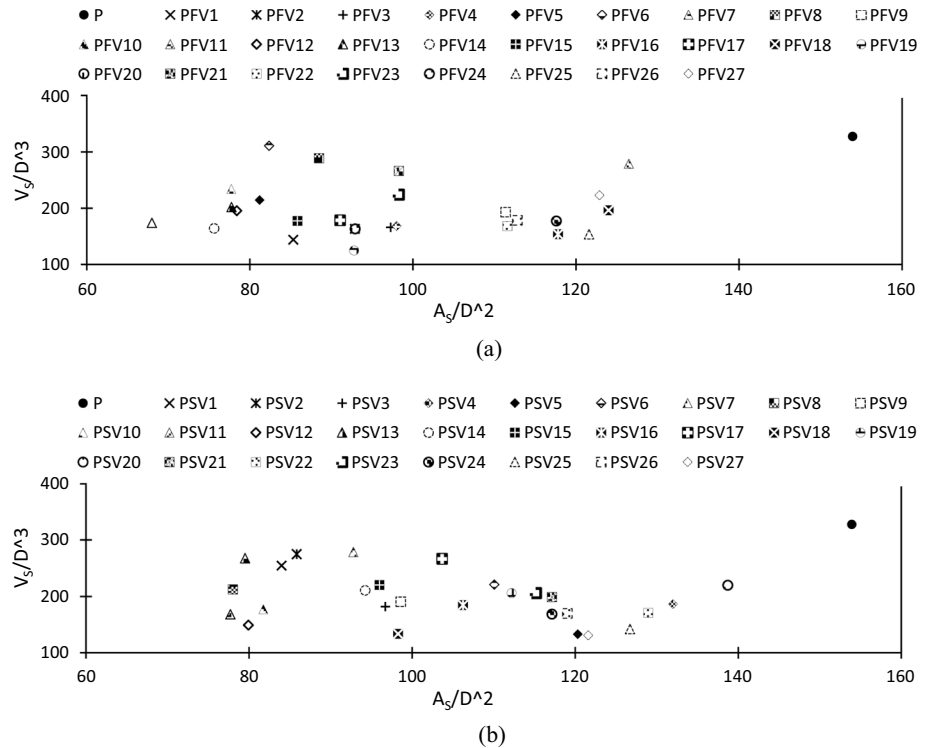


Fig. 16 The dimensionless area and volume of the scour cavity at the pier with vanes placed at a distance of **a** 0.4B and **b** 0.6B from the inner bank



overlapping vanes on changes in the length of the cavity is significant compared to the width of the cavity. The rectangle created over the scour cavity with submerged vanes had a length calculated in a range of 13.5–20D in every

model (Fig. 15a). In the models using submerged vanes at the distance of 0.6B from the inner bank, the width of the rectangle circumscribed over the scour cavity is between 5 and 7D. The rectangle circumscribed over the scour cavity

around the pier in PSV20 and PSV8, respectively, have the maximum and the minimum widths (Fig. 15b).

Figure 16 shows the scour cavity scope around the pier with a diagram illustrating the scour cavity area and volume around the bridge pier with the presence of the upstream submerged vanes, nondimensionalized with the second and third powers of the pier diameter in every model. It may be observed that the nondimensionalized area and volume of the scour cavity around the pier in P model are the largest among all the models with the presence of the submerged vanes, and these values are, respectively, $154D^2$ and $328D^3$. The largest nondimensionalized area occurs with the presence of the submerged vanes at a distance of $0.4B$ from the inner bank in PFV7, and the smallest in PFV11, with respective values of 126.5 and 68. Although PFV8, PFV16, and PFV17 models contributed little to reducing the maximum scour depth according to Table 2, they have resulted in, respectively, 42.5, 23.5, and 41% reductions in the area of the main scour cavity in comparison with P model according to Fig. 16a. Also, the minimum and maximum scour volumes around the pier occur with the presence of the submerged vanes in PFV19 and PFV6 arrangements with respective values of $125D^3$ and $311D^3$. It may be reasoned about PSV19 model that the smaller distance of the vanes from the pier shows that the water flow directs the sediments around the submerged vanes toward the bridge pier more strongly than in PSV6; hence, the scour around the pier develops less in the lateral and vertical axes. After PFV19, PFV1 arrangement had a better performance as it has resulted in a 55% reduction in the volume of the scour cavity in comparison with P model. Figure 16b indicates that the dimensionless zone of the scour cavity around the pier is the greatest in PSV20 and the smallest in PSV8. Comparing the maximum scour depth and cavity development at channel length and width showed different variation trends of these two parameters in some cases. For example, it may be concluded that despite the maximum scour depth around the pier in PSV10 model being greater than that in PSV25 (Table 2), the scour cavity reach around the pier in PSV10 is less than that in PSV25 according to Fig. 16b. In addition, the minimum volume of scour around the pier occurs in PSV27 arrangement with a value of $131D^3$. The data obtained from the simulations indicated that the variation trends in the scour cavity area and volume differ in a number of them. For example, the nondimensionalized scour cavity area at the pier of the PSV22 model is 17% greater than that in the PSV6 model; nevertheless, the volume of the scour cavity volume in PSV6 is 30% greater than that in PSV22.

The reduction percentages of the scour cavity area and volume in this model compared to the single-pier model are given in Table 3. As can be seen, the average reductions in the scour cavity area and volume are in the ranges of 9.88–55.82% and 5.15–61.94%, respectively. The effect of

Table 3 Reduction percentages of the scour cavity area and volume in comparison with those of the single-pier model

Run	Percentage of reduction (%)		Run	Percentage of reduction (%)	
	As	Vs		As	Vs
PFV1	44.57	56.07	PSV1	45.43	22.24
PFV2	39.66	50.19	PSV2	44.23	16.14
PFV3	36.80	49.38	PSV3	37.16	44.50
PFV4	36.33	48.68	PSV4	14.24	43.11
PFV5	47.25	34.56	PSV5	21.83	59.42
PFV6	46.49	5.15	PSV6	28.48	32.53
PFV7	17.83	14.85	PSV7	39.71	14.95
PFV8	42.52	11.88	PSV8	49.32	35.12
PFV9	27.65	41.04	PSV9	35.94	41.75
PFV10	49.51	28.55	PSV10	46.88	45.95
PFV11	55.82	46.99	PSV11	49.51	48.68
PFV12	49.06	40.31	PSV12	48.08	54.47
PFV13	49.48	38.42	PSV13	48.34	18.28
PFV14	50.88	49.90	PSV14	38.77	35.66
PFV15	44.23	45.89	PSV15	37.63	32.74
PFV16	23.47	53.12	PSV16	30.98	43.63
PFV17	40.83	45.53	PSV17	32.64	18.65
PFV18	19.44	40.10	PSV18	36.15	59.21
PFV19	39.71	61.94	PSV19	27.10	37.12
PFV20	39.63	50.19	PSV20	9.88	32.83
PFV21	36.15	18.76	PSV21	23.88	39.35
PFV22	27.49	48.68	PSV22	16.22	47.85
PFV23	36.15	31.65	PSV23	25.16	37.15
PFV24	23.60	45.89	PSV24	23.88	48.49
PFV25	21.00	53.12	PSV25	17.67	56.69
PFV26	26.72	45.53	PSV26	22.66	48.13
PFV27	20.17	32.01	PSV27	21.00	60.02
Average (%)	36.76	40.31	Average (%)	32.32	39.80

vanes on the reduction of scour cavity volume compared to its area was more evident. The scour cavity area and volume are averagely reduced by 34.5 and 40.1%, respectively. The reductions of the scour cavity volume in the experimental single-pier and triad-pier tests conducted by Safaripour et al. [21] were nearly 59 and 37% compared to their test with no submerged vane installed, respectively.

Conclusions

This study utilized the SSIIM numerical model to investigate the flow pattern around a cylindrical bridge pier located in a 180° bend. The objective was to examine the impact of submerged vanes on the mitigation of local scouring around the bridge pier and validate the findings with an experimental model. The variables considered in this study were the

location of submerged vanes across the channel width and their distances from the pier and from each other with the different 100, 50, and 0% overlapping lengths. The results obtained within the range of parameter alterations demonstrated that the SSIIM numerical model could accurately simulate scouring around the bridge pier with upstream submerged vanes in a sharp 180° bend. The scour cavity exhibited two distinct parts: one approaching the outer bank with less skewedness toward the downstream part and the other skewed one toward the inner bank due to vortices around the pier and the helical flow pattern. The presence of upstream submerged vanes resulted in a reduction in the scour depth around the bridge pier compared to the model without vanes. On average, the scour cavity area, volume, and scour depth were reduced by 9.88–55.82%, 5.15–61.94%, and 15.67–50.60%, respectively. The effect of the vanes on reducing the scour cavity length compared to its width was particularly noticeable. The presence of submerged vanes installed at the upstream side of the bridge pier resulted in a scour cavity with a reduced slope in both downstream and upstream directions, as well as orientations toward the inner and outer banks. The installation of submerged vanes at the upstream side of the bridge pier led to a more symmetrical scour cavity slope compared to the single-pier model. The rectangular shape formed around the scour cavity with the presence of submerged vanes had a length ranging from 13.5 to 20D. The reduced width and length of the rectangular shape, as well as the decreased scour cavity area and volume at the bridge pier, were attributed to the installation of submerged vanes. The influence of changes in the length of overlapping vanes on alterations in the scour cavity length compared to its width was found to be significant.

Funding The authors declare that no funds, grants, or other supports were received during the preparation of this manuscript.

Availability of data and materials Data are available on request.

Declarations

Conflict of interest The authors have no relevant financial or non-financial interests to disclose.

Ethical approval This paper neither was published nor is under review elsewhere.

Consent to participate The authors declare their consent for participating in this work.

Consent for publication The authors have participated in the preparation or submission of this paper for publication in Innovative Infrastructure Solutions.

References

- Ye J, McCorquodale JA (1998) Simulation of curved open channel flows by 3D hydrodynamic model. *J Hydraul Eng* 124(7):687–698. [https://doi.org/10.1061/\(ASCE\)0733-9429\(1998\)124:7\(687\)](https://doi.org/10.1061/(ASCE)0733-9429(1998)124:7(687))
- Wu W, Rodi W, Wenka T (2000) 3D numerical modeling of flow and sediment transport in open channels. *J Hydraul Eng* 126(1):4–15. [https://doi.org/10.1061/\(ASCE\)0733-9429\(2000\)126:1\(4\)](https://doi.org/10.1061/(ASCE)0733-9429(2000)126:1(4))
- Kassem AA, Chaudhry MH (2002) Numerical modeling of bed evolution in channel bends. *J Hydraul Eng* 128(5):507–514. [https://doi.org/10.1061/\(ASCE\)0733-9429\(2002\)128:5\(507\)](https://doi.org/10.1061/(ASCE)0733-9429(2002)128:5(507))
- Wilson CAME, Boxall JB, Guymer I, Olsen NRB (2003) Validation of a three-dimensional numerical code in the simulation of pseudo-natural meandering flows. *J Hydraul Eng* 129(10):758–768. [https://doi.org/10.1061/\(ASCE\)0733-9429\(2003\)129:10\(758\)](https://doi.org/10.1061/(ASCE)0733-9429(2003)129:10(758))
- Wildhagen J (2004) Applied computational fluid dynamics with sediment transport in a sharply curved meandering channel. Institute for Hydromechanics University of Karlsruhe (TH), Germany
- Aghaee Y, Hakimzadeh H (2010) Three dimensional numerical modeling of flow around bridge piers using LES and RANS. *River Flow*, 211–218. <https://hdl.handle.net/20.500.11970/99648>
- Naji Abhari M, Ghodsian M, Vaghefi M, Panahpur N (2010) Experimental and numerical simulation of flow in a 90 bend. *Flow Meas Instrum* 21(3):292–298. <https://doi.org/10.1016/j.flowmeasinst.2010.03.002>
- Ghobadian R, Mohammadi K (2011) Simulation of subcritical flow pattern in 180 uniform and convergent open-channel bends using SSIIM 3-D model. *Water Sci Eng* 4(3):270–283. <https://doi.org/10.3882/j.issn.1674-2370.2011.03.004>
- Nekoufar K, Kouhpari H (2013) Control and decrease the scouring of bridge pier by method of non-submerged plates using SSIIM software. *Acta Technica Corviniensis-Bull Eng* 6(4):35
- Abdallah Mohamed Y, Hemdan Nasr-Allah T, Mohamed Abdel-Aal G, Shawky Awad AS (2014) Investigating the effect of curved shape of bridge abutment provided with collar on local scour, experimentally and numerically. *Ain Shams Eng J* 6(2):403–411. <https://doi.org/10.1016/j.asej.2014.10.011>
- Akib S, Bassar H, Karami H, Jahangirzadeh A (2014) Retrofitting of bridge piers against the scour damages: case study of the Marand-Soofian route bridge. *World Acad Sci, Eng Technol, Int J Civ, Archit Sci Eng* 8:56–60. <https://doi.org/10.5281/zenodo.1336432>
- Ehteram M, Meymand AM (2015) Numerical modeling of scour depth at side piers of the bridge. *J Comput Appl Math* 280:68–79. <https://doi.org/10.1016/j.cam.2014.11.039>
- Bassar H, Cheraghi R, Karami H, Ardeshir A, Amir Mojahedi M, Akib S, Shamsheirband S (2015) Modeling sediment transport around a rectangular bridge abutment. *Environ Fluid Mech* 15(6):1105–1114. <https://doi.org/10.1007/s10652-015-9398-z>
- Ghobadian R, Basiri M (2016) The effect of downstream curved edge on local scouring at 60-degree open channel junction using SSIIM1 model. *Ain Shams Eng J* 7(2):543–552. <https://doi.org/10.1016/j.asej.2015.06.001>
- Azizi S, Farsadzadeh D, Arvanaghi H, Abbaspour A (2016) Numerical simulation of flow pattern around the bridge pier with submerged vanes. *J Hydraul Struct* 2(2):46–61. <https://doi.org/10.22055/JHS.2016.12856>
- Ouyang HT, Lin CP (2016) Characteristics of interactions among a row of submerged vanes in various shapes. *J Hydro-Environ Res* 13:14–25. <https://doi.org/10.1016/j.jher.2016.05.003>
- Johnson PA, Hey RD, Tessier M, Rosgen DL (2001) Use of vanes for control of scour at vertical wall abutments. *J Hydraul Eng ASCE* 127(9):772–778. [https://doi.org/10.1061/\(ASCE\)0733-9429\(2001\)127:9\(772\)](https://doi.org/10.1061/(ASCE)0733-9429(2001)127:9(772))

18. Parchami L, Asghari Pari S, Shafai Bajestan M (2016) Experimental investigation of submerged vanes shape effect on bridge pier scouring. *J Water Soil Knowl* 27(1):29–41 ((In Persian))
19. Vaghefi M, Safaripour N, Zarei E, Mahmoudi A, Hashemi S (2018) Experimental investigation on the effect of overlapping upstream submerged vanes on bend topography with a bridge pier. *Modares Civ Eng J (M.C.E.J)* 15(2):245–255 ((In Persian))
20. Zarei E, Vaghefi M, Sh HS (2019) Bed topography variations in bend by simultaneous installation of submerged vanes and single bridge pier. *Arab J Geosci* 12(6):1–10. <https://doi.org/10.1007/s12517-019-4342-z>
21. Safaripour N, Vaghefi M, Mahmoudi A (2020) Experimental study of the effect of submergence ratio of double submerged vanes on topography alterations and temporal evaluation of the maximum scour in a 180-degree bend with a bridge pier group. *Int J River Basin Manag* 20(4):427–441. <https://doi.org/10.1080/15715124.2020.1837144>
22. Dey L, Barbhuiya AK, Biswas P (2017) Experimental study on bank erosion and protection using submerged vane placed at an optimum angle in a 180° laboratory channel bend. *Geomorphology* 283:32–40. <https://doi.org/10.1016/j.geomorph.2017.01.022>
23. Karimi N, Heidarnejad M, Masjedi A (2017) Scour depth at inclined bridge piers along a straight path: a laboratory study. *Eng Sci Technol, Int J* 20(4):1302–1307. <https://doi.org/10.1016/j.jestch.2017.07.004>
24. Hamidi A, Siadatmousavi SM (2018) Numerical simulation of scour and flow field for different arrangements of two piers using SSIIM model. *Ain Shams Eng J* 9(4):2415–2426. <https://doi.org/10.1016/j.asej.2017.03.012>
25. Vaghefi M, Safaripour Y, Akbari M (2017) Numerical comparison of the parameters influencing the turbulent flow using a T-shaped spur dike in a 90° bend. *J Appl Fluid Mech* 10(1):231–241. <https://doi.org/10.18869/ACADPUB.JAFM.73.238.26175>
26. Khayyun TS, Mouhamed NH (2018) Three dimensional modeling of sediment transport upstream of Al-Betera regulator-Iraq. *J Eng Sustain Dev* 22(5):215–238. <https://doi.org/10.31272/jesd.2018.5.16>
27. Hammerling M, Walczak N, Nowak A, Mazur R, Chmista J (2019) Modelling velocity distributions and river bed changes using computer code SSIIM below sills stabilizing the riverbed. *Pol J Environ Stud* 28(3):1165–1179. <https://doi.org/10.15244/pjoes/85224>
28. Asadollahi M, Vaghefi M, Tabib Nazhad Motlagh MJ (2019) Experimental and numerical comparison of flow and scour patterns around a single and triple bridge piers located at a sharp 180 degrees bend. *Scientia Iranica* 28(1):1–14. <https://doi.org/10.24200/sci.2019.5637.1391>
29. Rasaei M, Nazari S, Eslamian S (2020) Experimental and numerical investigation the effect of pier position on local scouring around bridge pier at a 90° convergent bend. *J Hydraul Struct* 6(1):55–76. <https://doi.org/10.22055/JHS.2020.32753.1134>
30. Asadollahi M, Vaghefi M, Akbari M (2020) Effect of the position of perpendicular pier groups in a sharp bend on flow and scour patterns: numerical simulation. *J Braz Soc Mech Sci Eng* 42(8):1–15. <https://doi.org/10.1007/s40430-020-02503-2>
31. Ben Mohammad Khajeh S, Vaghefi M (2020) Investigation of abutment effect on scouring around inclined pier at a bend. *J Appl Water Eng Res* 8(2):125–138. <https://doi.org/10.1080/23249676.2020.1761898>
32. Moghanloo M, Vaghefi M, Ghodsian M (2020) Experimental study on the effect of thickness and level of the collar on the scour pattern in 180° sharp bend with bridge pier. *Iran J Sci Technol, Trans Civ Eng* 44(5):1–19. <https://doi.org/10.1007/s40996-020-00511-9>
33. Sedighi F, Vaghefi M, Ahmadi G (2020) The effect of inclined pair piers on bed topography: clear water, incipient motion and live bed. *Iran J Sci Technol, Trans Civ Eng* 45:1871–1890. <https://doi.org/10.1007/s40996-020-00481-y>
34. Abdi Chooplou C, Vaghefi M, Safaripour Y (2021) Numerical simulation of the flow pattern around a single bridge pier with upstream of submerged vanes in sharp 180-degree bend with an alluvial bed under the influence of submerged vanes and the bridge pier. *MCEJ* 21(6):88–98
35. Vaghefi M, Moradi S, Abdi Chooplou Ch (2021) Numerical study of bed topography variations owing to placement of triad series of vertical bridge piers installed in a 180-degree bend with different relative radii using SSIIM numerical model. *Iran J Sci Technol, Trans Civ Eng* 45(3):1971–1988. <https://doi.org/10.1007/s40996-020-00559-7>
36. Chauhan V, Singhal GD, Chavan R (2022) A review of sediment deflection in rivers using submerged vanes. *ISH J Hydraul Eng.* <https://doi.org/10.1080/09715010.2022.2084352>
37. Sadeqlu M, Hamidi M (2022) Numerical investigation of the cylindrical bridge pier scour reduction by installing a group of two submerged vanes. *Irrig Drain Struct Eng Res* 22(85):91–114. <https://doi.org/10.22092/idsr.2022.357739.1502>
38. Biswal SK, Das A (2022) Numerical modelling of scour and flow field for two different arrangements of piers using SSIIM model. *Int Symp Hydraul Struct.* <https://doi.org/10.26077/6756-2055>
39. Harshvardhan H, Kaushal DR (2022) CFD modelling of local scour around a bridge pier. In: AGU fall meeting abstracts. 2022AGUFM.H22N0982H. 2022:H22N-0982
40. Abdi Chooplou C, Vaghefi M, Akbari M (2023) Effect of repositioned submerged vanes on local scour variations around a pier in a bend: experimental investigation. *Int J Environ Sci Technol.* <https://doi.org/10.1007/s13762-023-05031-3>
41. Majedi-Asl M, Kouhdaragh M, Fuladipannah M (2023) Mapping scour depth around group bridge pier under controlled conditions. *J Hydraul Struct* 8(4):57–72. <https://doi.org/10.22055/JHS.2023.43132.1243>
42. Fathi A, Zomorodian SA, Zolghadr M, Chadee A, Chiew YM, Kumar B, Martin H (2023) Combination of riprap and submerged vane as an abutment scour countermeasure. *Fluids* 8(2):41. <https://doi.org/10.3390/fluids8020041>
43. Niknezhad F, Mahmoudi A, Vaghefi M (2023) A study of the effects of a lateral intake's positions on the flow pattern around a bridge pier in a 180° bend using SSIIM2. *Arab J Sci Eng.* <https://doi.org/10.1080/15715124.2023.2167824>
44. Okhravi S, Gohari S, Alemi M, Maia R (2023) Numerical modeling of local scour of non-uniform graded sediment for two arrangements of pile groups. *Int J Sedim Res.* <https://doi.org/10.1016/j.ijsrc.2023.04.002>
45. Sarlak H, Bejestan MS, Sajjadi SM (2023) Experimental investigation of the effect of permeability and angle of gabion submerged vane on bed topography. *Arab J Geosci* 16(4):288. <https://doi.org/10.1007/s12517-023-11332-1>
46. Leschziner MA, Rodi W (1979) Calculation of strongly curved open channel flow. *J Hydraul Div* 105(10):1297–1314
47. Olsen NRB (2014) A three-dimensional numerical model for simulation of sediment movement in water intakes with multi-block option, Department of Hydraulic and environmental Engineering, Norwegian University of Science and Technology, User's manual, Norway, 172–183
48. Van Rijn LC (1987) Mathematical modeling of morphological processes in the case suspended sediment transport. PHD thesis. Delft University of Technology, 97–99
49. Neill CR (1967) Mean-velocity criterion for scour of coarse uniform bed-material. Paper presented at the 12th Congress of the international association for hydraulics research, Colorado, U.S.A
50. De Medeiros IC, da Costa Silva JFCB, Silva RM, Santos CAG (2019) Run-off-erosion modelling and water balance in the Epitácio Pessoa Dam river basin, Paraíba State in Brazil. *Int J*

- Environ Sci Technol 16:3035–3048. <https://doi.org/10.1007/s13762-018-1940-3>
51. Chiew YM, Melville BW (1987) Local scour around bridge piers. *J Hydraul Res* 25(1):15–26
 52. Amini A, Mohammad TA (2017) Local scour prediction around piers with complex geometry. *Mar Georesour Geotechnol* 35(6):857–864. <https://doi.org/10.1080/1064119X.2016.1256923>
 53. Odgaard AJ, Wang Y (1991) Sediment management with submerged vanes. I. theory. *J Hydraul Eng ASCE* 117(3):267–283
 54. Raudkivi AJ, Ettema R (1983) Clear-water scour at cylindrical piers. *J Hydraul Eng* 125:59–66
 55. Raudkivi AJ (1998) *Loose boundary hydraulics*. Balkema, Brookfield
 56. Ahmad Z (2013) Prediction of longitudinal dispersion coefficient using laboratory and field data: relationship comparisons. *Hydrol Res* 44(2):362–376. <https://doi.org/10.2166/nh.2012.047>

Springer Nature or its licensor (e.g. a society or other partner) holds exclusive rights to this article under a publishing agreement with the author(s) or other rightsholder(s); author self-archiving of the accepted manuscript version of this article is solely governed by the terms of such publishing agreement and applicable law.